Applied Catalysis B: Environmental 108–109 (2011) 6–13

Contents lists available at ScienceDirect

Applied Catalysis B: Environmental

journal homepage: www.elsevier.com/locate/apcatb

Hydrogen production from biomass gasification with Ni/MCM-41 catalysts: Influence of Ni content

Chunfei Wu [a], Leizhi Wang [b], Paul T. Williams [a,*], Jeffrey Shi [b], Jun Huang [b,**]

[a] Energy & Resources Research Institute, The University of Leeds, Leeds, LS2 9JT, UK
[b] Laboratory for Catalysis Engineering, School of Chemical and Biomolecular Engineering, The University of Sydney, NSW 2006, Australia

ARTICLE INFO

Article history:
Received 26 May 2011
Received in revised form 18 July 2011
Accepted 19 July 2011
Available online 26 July 2011

Keywords:
Biomass
Pyrolysis
Gasification
Ni/MCM-41
Two-stage fixed bed reactor

ABSTRACT

The steam pyrolysis-gasification of biomass, wood sawdust, was carried out with a Ni/MCM-41 catalyst for hydrogen production in a two-stage fixed bed reaction system. The wood sawdust was pyrolysed in the first reactor and the derived products were gasified in the second reactor. The synthesised MCM-41 mesoporous catalyst supports were impregnated with different Ni loadings (5, 10, 20 and 40 wt.%), which were characterized with X-ray diffraction (XRD), scanning electron microscopy (SEM), temperature programmed reduction (TPR), transmission electron microscopy (TEM) and temperature-programmed oxidation (TPO). NiO particles were homogeneously dispersed inside the pores of 5, 10, and 20 wt.% Ni/MCM-41 catalysts; however, more bulkly NiO particles (up to 200 nm particle size) were detected outside the pores with an increase of the Ni loading up to 40 wt.%. Gas production was increased from 40.7 to 62.8 wt.%, hydrogen production was increased from 30.1 to 50.6 vol.% of total gas composition when the Ni loading was increased from 5 to 40 wt.% during the pyrolysis-gasification of wood sawdust. This work showed low coke deposition (from 0.5 to 4.0 wt.%) with valuable bio-oil by-products using the Ni/MCM-41 catalyst. The highly efficient conversion of renewable biomass resource to hydrogen and bio-oil with very low coke deposition indicates that biomass gasification on Ni/MCM-41 catalysts via two-stage reaction is a promising method for the development of the biorefinery concept.

1. Introduction

Hydrogen is regarded as a clean fuel for low carbon energy systems [1–3]. The use of hydrogen for power generation in fuel cells and as a transport fuel has been identified. In addition, hydrogen will be the energy carrier from other resources such as hydropower, wind, solar and biomass. At present, hydrogen is largely produced either from fossil fuel sources such as natural gas, naphtha and coal or via water electrolysis, photolysis or thermolysis [4–6]. The use of fossil fuels has caused major pressures in regard to energy security and environmental impact, due to the depletion of resources and the release of green-house gases. Therefore, it is essential to find a renewable feedstock for the production of hydrogen for sustainable development. Producing hydrogen from gasification of biomass wastes, particularly in the presence of steam, represents a promising route to produce this clean and CO_2-neutral fuel [7,8]. The main advantage of biomass gasification is that a wide range of cheap and non-food feedstocks are available, including agricultural residues, forestry residues, by-products from biorefineries and wastes from the food industry such as brewery wastes and the biodegradable and plastic fractions of municipal solid waste [9–11].

To enhance hydrogen production, many catalysts have been researched for biomass gasification [9,10]. Among them, supported Ni-catalysts have been extensively reported to be effective for hydrogen production from biomass gasification [12–14], and additionally are lower cost compared to noble metal catalysts. Generally, supports for Ni-catalysts have a large influence on the catalytic properties of their metal active centres due to various interactions between supports and metal particles. Therefore, different supports have been studied for Ni-catalysts in biomass gasification. For example, Al_2O_3 has been commonly investigated as a Ni support due to its chemical and physical stability [15,16]. MgO has been reported to exhibit high catalytic activity during steam reforming of naphthalene as a model compound of biomass tar [17]. In addition, CeO_2 [16], dolomite [18], olivine [19], and zeolites [20,21] have also been investigated as Ni supports for biomass gasification. However, a challenge for the improvement of biomass catalytic gasification efficiency is coke formation since coke deposition on catalytic active sites causes the deactivation of the catalyst and the gas yield is reduced due to carbon deposition.

Srinakruang et al. [15] reported that Ni/dolomite catalyst showed less carbon deposition compared with Ni/Al_2O_3 catalyst,

* Corresponding author. Tel.: +44 1133432504.
** Corresponding author. Tel.: +61 29351 7483.
E-mail addresses: p.t.williams@leeds.ac.uk (P.T. Williams), jun.huang@sydney.edu.au (J. Huang).

0926-3373/$ – see front matter © 2011 Published by Elsevier B.V.
doi:10.1016/j.apcatb.2011.07.023

Table 1
Proximate and ultimate analysis of the wood sawdust.

	Proximate analysis (wt.%)			
	Moisture	Volatile	Fixed carbon	Ash
Wood Sawdust	6.4	74.8	18.3	1.2
	Ultimate analysis[a] (wt.%)			
	C	H	O	N
Wood Sawdust	47.1	5.9	46.9	0.1

[a] Oxygen content was calculated by mass difference.

when toluene was used as a model compound of tar. The Ni/Al_2O_3 catalyst has also been found to be easily deactivated during the pyrolysis-gasification of polypropylene [3]. It was also reported that Ni/MgO had less coke deposition but with a lower hydrogen production. Inaba et al. [21] reported that a Ni/CeO_2 catalyst experienced lowered carbon deposition during the gasification of cellulose, however, the Ni/CeO_2 catalyst showed lower hydrogen production compared with a Ni/H-ZSM-5 catalyst. Additionally, the Ni/H-ZSM-5 catalyst had a higher carbon deposition. They concluded that the Ni/Ce/H-ZSM-5 was a promising non-nobel-metal catalyst for hydrogen production for the cellulose gasification process [21].

Compared with microporous H-ZSM-5, mesoporous supports have a higher surface area (around 1000 $m^2\,g^{-1}$) with larger pore size (2–10 nm diameter), which are potential depositories for Ni nano-particles. However, recent efforts using thermogravimetric-mass spectrometer (TG-MS) as a reaction and analysis system reported low gas and hydrogen production even for gasification of a biomass model compound (cellulose) on supported Ni on mesoporous materials [22,23].

Two-stage reaction systems have been extensively used for investigation of the gasification process, due to the advantages of easy control of temperature of each stage of the process, the potential for catalyst recycling and increasing contacts between derived pyrolysis products and catalyst [3,7,21].

In this work, a two-stage pyrolysis-gasification reactor was used to test the catalytic performance of newly prepared Ni/MCM-41 catalysts for gasification of wood sawdust. Since Ni or NiO particle size on the supports is an important factor for the gasification of biomass, the influence of Ni content in relation to the particle size distribution was investigated, which further influences hydrogen production and coke deposition.

2. Materials and experimental

2.1. Materials

Wood sawdust with a size less than 0.2 mm was used in this work. The elemental analysis and proximate analysis results are shown in Table 1. The sample shows a moisture content of 6.4 wt.%, volatile content of 74.8 wt.%, fixed carbon of 18.3 wt.% and an ash content of 1.2 wt.%. In addition, C, H, O and N content was 47.1, 5.9, 46.9 and 0.1 wt.%, respectively.

The MCM-41 support was prepared according to the procedures reported by Cheng et al. [24]. Different Ni loadings (5, 10, 20 and 40 wt.%) on MCM-41 were prepared by an impregnation method. Initially, the required amount of $Ni(NO_3)_2{\cdot}6H_2O$ (Sigma–Aldrich) was dissolved in ethanol (99%, Sigma–Aldrich) to form a 1 mol/l of solution. Then impregnation was employed by addition of powdered MCM-41 to the nickel precursor solution. The mixture was stirred for 2 h followed by evaporation of the mixture at 80 °C. The obtained solids were calcined in a muffle furnace at 550 °C for 4 h with a heating rate of 1 °C min^{-1} in the presence of static air.

2.2. Gasification

Pyrolysis-gasification in the presence of the prepared Ni/MCM-41 catalysts was carried out with a two-stage fixed-bed reaction system. The wood sawdust was initially pyrolysed in the first reactor, and then the derived products were gasified in the second reactor. The schematic diagram of the reactor system was presented in our previous work [3].

During the experiment, about 0.8 g of wood sawdust was placed in the first reactor and 0.25 g of Ni/MCM-41 catalyst (or sand for blank experiments) in the second reactor. The temperatures of the two reactors were controlled separately. The temperature of the catalyst bed was initially increased and stabilized at 800 °C. Then the first reactor (pyrolysis) was started to be heated up to 550 °C with a heating rate of 40 °C min^{-1}. Water was injected with a flow rate of 5.0 ml h^{-1} by a syringe pump when the pyrolysis temperature reached at around 200 °C. The experiment was found to be almost complete with a total time of 40 min after the start of heating the first reactor (pyrolysis). The generated products from the second reactor were condensed with an air-cool condenser and a dry-ice cooled condenser. The non-condensed gases were collected by a 25 l Tedlar™ gas bag.

2.3. Analysis of gas and oil

Concentrations of the gases collected in the sample bag were analysed off-line by packed column gas chromatography (GC). C_1 to C_4 hydrocarbons were analysed using a Varian 3380 gas chromatograph with a flame ionisation detector, with an 80–100 mesh Hysep column and nitrogen carrier gas. Hydrogen, oxygen, carbon monoxide and nitrogen were analysed with a Varian 3380 GC on a 60–80 mesh molecular sieve column with argon carrier gas, whilst carbon dioxide was analysed by another Varian 3380 GC on a Hysep 80–100 mesh column with argon carrier gas.

The liquid products including oil and un-reacted water from the condensers were collected in the presence of wash-agent dichloromethane (DCM). The liquid mixture was first filtered with a bed of anhydrous sodium sulphate to eliminate the water content, and the oil was further diluted with DCM to a detectable level. The oil samples in DCM were analysed with gas chromatograph/mass spectrometry (GC/MS). The GC/MS was a Hewlett Packard 5280 gas chromatograph coupled to a HP5271 ion trap mass selective detector (GC/MS) with on-column auto-injection. The ion-mass spectra derived were automatically compared to spectral libraries using HP Chemstation software and similarity indexes (SI) of >70% were reliably used to identify compounds.

2.4. Characterization of fresh and used catalysts

X-ray diffraction (XRD) patterns of the prepared fresh catalysts were obtained on a SIEMENS D5000 in the range of 1.5–70° with a scanning step of 0.02° using Cu Kα radiation (0.1542 nm wavelength).

The surface area, average pore size, and total pore volume of the fresh Ni/MCM-41 catalysts were determined by N_2 adsorption and desorption isotherms on Quantachrome Autosorb-1. Before the isotherms analysis, 50 mg of each catalyst was degassed under vacuum at 110 °C for 12 h.

Scanning electron microscopy (SEM) (FESEM, Zeiss Ultra+) was used to analyze the fresh catalysts. Another SEM (LEO 1530)

Table 2
Surface properties of fresh Ni/MCM-41 catalysts.

Catalyst	Surface area ($m^2\ g^{-1}$)	Total pore volume ($cm^3\ g^{-1}$)	Average pore size (nm)
5 wt.% Ni/MCM-41	1081	0.785	2.90
10 wt.% Ni/MCM-41	868	0.629	2.90
20 wt.% Ni/MCM-41	869	0.612	2.82
40 wt.% Ni/MCM-41	737	0.496	2.69

coupled to an energy dispersive X-ray spectroscope (EDXS) was used to characterize the used Ni/MCM-41 catalysts.

Temperature programmed reduction (TPR) of the prepared Ni/MCM-41 catalysts were carried out using a modified thermogravimetric analyser (SDT Q600) coupled with a mass spectrometer (ThermoStar GSD301). Ni-MCM-41 catalysts were loaded in an alumina pan and placed in the TGA furnace. Prior to the commencement of each experiment the sample was heated at 20 °C min^{-1} with pure N_2 (500 ml/min) from room temperature to 500 °C, in order to remove the water inside the pores of the catalysts. After water removal, the furnace reaction area was purged by a flow containing 5% H_2 and 95% Ar (500 ml/min) for 1 h. During the reduction process, variance of generated gas and mass loss were respectively monitored by the MS and TGA through a heated capillary delivery. The catalysts were heated from room temperature to 1000 °C at a rate of 10 °C min^{-1}.

Fresh Ni/MCM-41 catalysts were characterized by a Transmission electron microscopy (TEM) employed using a Philips CM120 BioFilter. The reacted Ni/MCM-41 catalysts were characterized with another TEM (Philips CM200).

The temperature-programmed oxidation (TPO) of the reacted catalysts was carried out using a Stanton-Redcroft thermogravimetric analyser (TGA and DTG) to determine the properties of the coked carbons deposited on the reacted catalysts. About 10 mg of the reacted catalyst was heated in an atmosphere of air at 15 °C min^{-1} to a final temperature of 800 °C, with a dwell time of 10 min.

3. Results and discussions

3.1. Characterization of fresh Ni/MCM-41 catalysts

3.1.1. N_2 adsorption/desorption analysis of fresh Ni/MCM-41 catalysts

The results of gas physical adsorption/desorption for the fresh Ni/MCM-41 catalysts are presented in Table 2 and Fig. 1. Higher surface area (>737 $m^2\ g^{-1}$) and pore volume (>0.496 $cm^3\ g^{-1}$) were obtained. In addition, average pore size (2.69–2.90 nm) with a narrow pore size distribution was found for these catalysts (Fig. 1a). From Table 2, surface area, total pore volume and average pore size seemed to be reduced with the increase of Ni loading from 5 to 40 wt.% in the Ni/MCM-41 catalyst. N_2 adsorption/desorption isotherms (Fig. 1b) have shown that Ni/MCM-41 catalysts prepared in this work are mesoporous materials.

3.1.2. XRD analysis of fresh Ni/MCM-41 catalysts

The XRD analysis (Fig. 2) showed that all the samples exhibited a broad amorphous silica peak at around 23°. The XRD pattern of 40 wt.% Ni/MCM-41 showed three narrow and strong peaks at 37°, 43° and 64°, which were assigned to NiO(1 0 1), NiO(0 1 2) and NiO(1 1 0) on bulk NiO particles, respectively [25]. The XRD pattern of 20 wt.% Ni/MCM-41 exhibited broad and weak diffraction peaks at similar positions. It suggests that the NiO particles are smaller on the 20 wt.% Ni/MCM-41 catalyst compared with those on the 40 wt.% Ni/MCM-41 catalyst. However, these peaks were difficult to observe on the 5 and 10 wt.% Ni/MCM-41 catalysts. It is

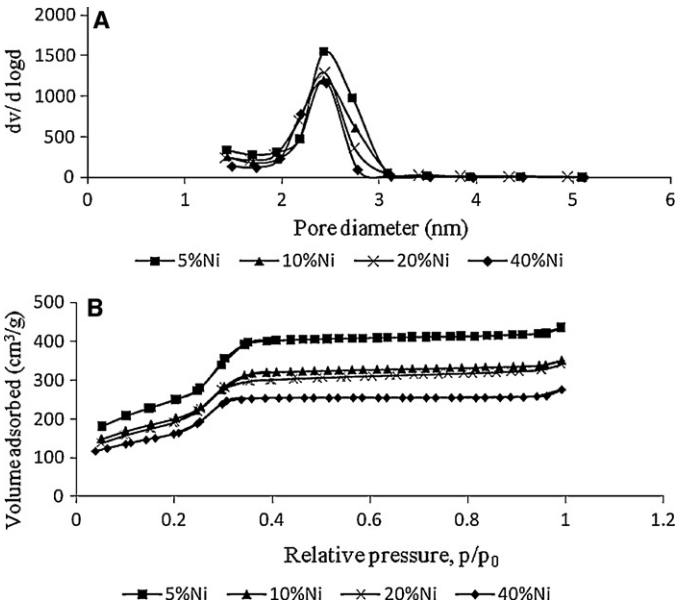

Fig. 1. Pore size distribution (a) and N_2 adsorption/desorption isotherms of the fresh catalysts (b).

suggested that nearly all NiO particles on the 5 and 10 wt.% Ni/MCM-41 and most NiO particles on the 20 wt.% Ni/MCM-41 catalysts were located inside nano-pores of the MCM-41 [26]. Increasing the loading of Ni from 20 to 40 wt.% on the supports, showed that the NiO particle size was increased due to the reduction of peak width according to the Scherrer equation. This phenomenon was also obtained from the SEM analysis.

3.1.3. SEM and TEM characterization of fresh Ni/MCM-41 catalysts

From the SEM images (Fig. 3), the morphology of the Ni/MCM-41 is well-ordered with a diameter size of about 200–500 nm for the MCM-41 support. As shown in Fig. 3(a) and (b), the bulk nickel oxides could not be observed on the MCM-41 surface. Increasing the Ni loading, Fig. 3(c) showed a small amount of bulk NiO

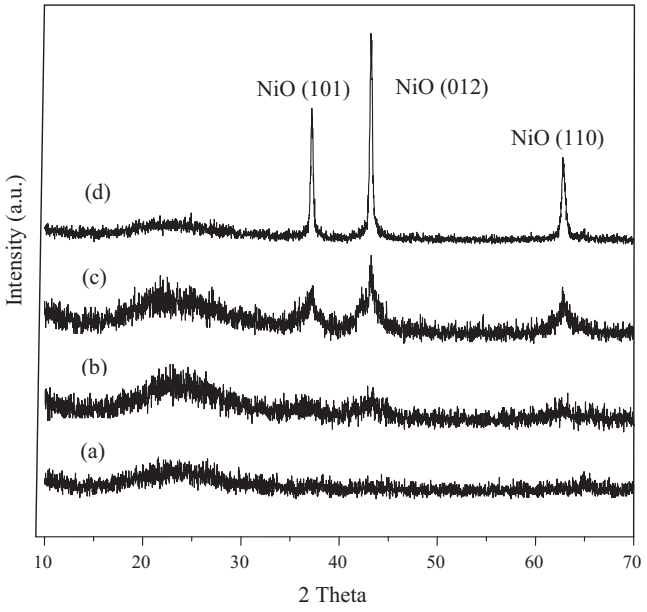

Fig. 2. XRD analysis of fresh Ni/MCM-41 catalysts; (a): 5 wt.% Ni/MCM-41; (b): 10 wt.% Ni/MCM-41; (c): 20 wt.% Ni/MCM-41; (d): 40 wt.% Ni/MCM-41.

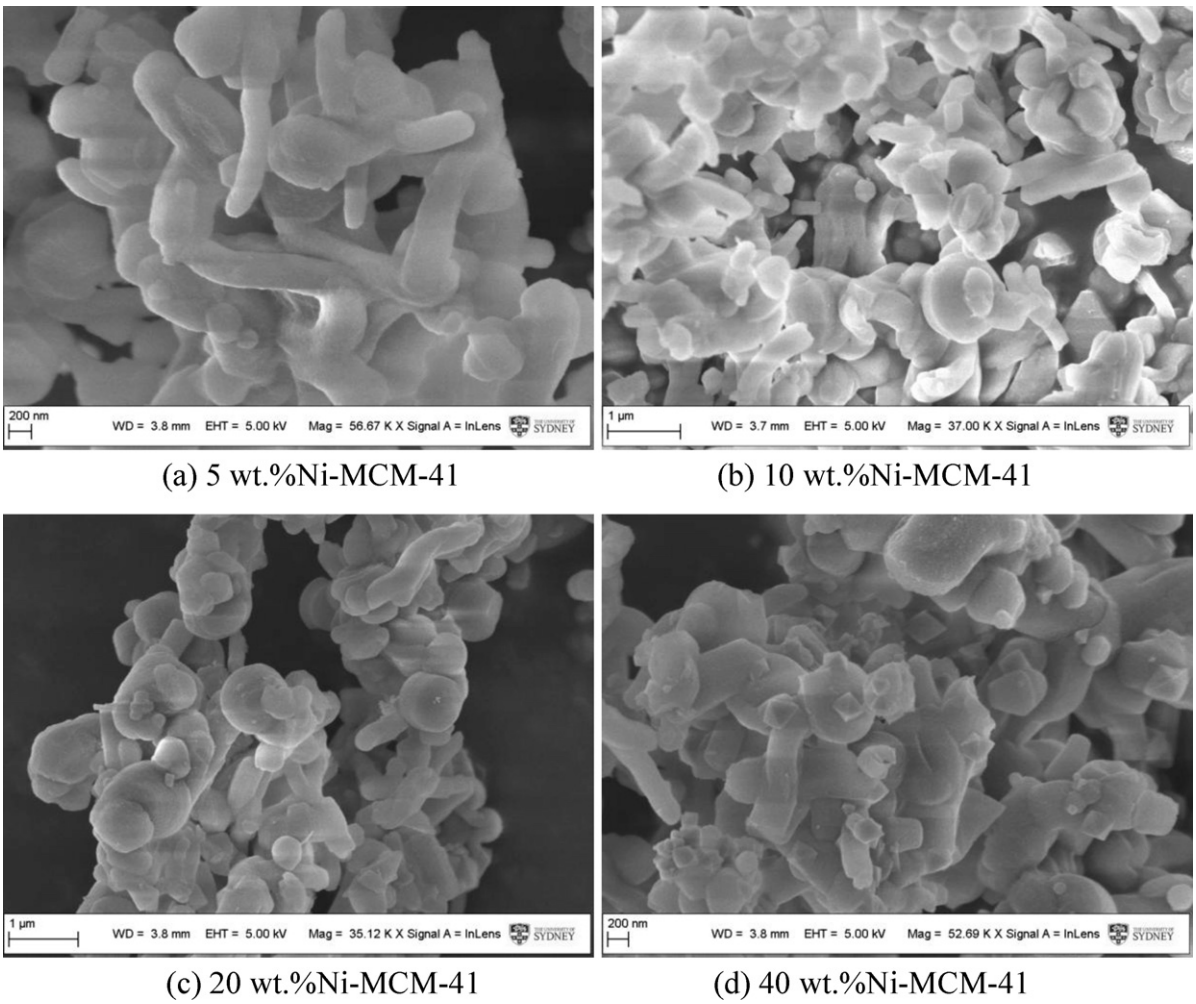

Fig. 3. SEM results of fresh Ni/MCM-41 catalysts.

particles occurred on the external surface of the 20 wt.% Ni/MCM-41. For the 40 wt.% Ni/MCM-41 catalyst (Fig. 3(d)), the size of the bulk NiO particles was increased up to 200 nm and more of these metal particles were accumulated on the external surface.

TEM images in Fig. 4 show that most of the loaded NiO in the 20 wt.% Ni/MCM-41 prepared catalyst were small particles (less than 3 nm) and were well distributed inside the pores of the MCM-41. Furthermore, bulk NiO particles (up to 200 nm) were clearly obtained for the 40 wt.% Ni/MCM-41 catalyst (Fig. 3). For a 10 wt.% Ni/Al_2O_3 catalyst prepared by Li et al. [27], the Ni particle size was found to be between 10 and 20 nm for the reduced catalyst. A 5.9 wt.% Ni/MCM-41 catalyst prepared by impregnation of nickel on MCM-41 was reported to have a Ni particle size around 6.7 nm [28]. In addition, various Ni/zeolite catalysts were prepared by Inaba et al. [21], a Ni particle size between 20 and 30 nm was reported. Therefore, the Ni/MCM-41 catalyst with Ni loading from 5 to 20 wt.% prepared in this work, appeared to have a better Ni dispersion compared to the Ni-catalysts prepared by others reported in the literature [21,27,28].

3.1.4. TPR analysis of the fresh catalysts

Fig. 5 shows the results of weight loss intensity of the fresh catalyst against temperature during TPR analysis. In the case of the 40 wt.% Ni/MCM-41 catalyst (Fig. 5d), two main peaks were observed. The larger low-temperature peak at about 390 °C is suggested to be the reduction of the bulk NiO presented on the outside of the pores of the catalysts; the observation has been supported by the SEM analysis (Fig. 3) [29,30]. However, the low-temperature peak becomes much smaller for the 20 wt.% Ni/MCM-41 catalyst, and almost disappeared for the 10 wt.% Ni/MCM-41 and 5 wt.% Ni/MCM-41 catalysts. It suggests that the amount of bulk NiO particles located on the surface of the support decreased sharply by reducing the Ni loading. In addition, the first reduction peak for the bulk NiO particles shifts from around 320 to 360 °C (Fig. 5) with increasing Ni loading, indicating larger bulk NiO crystals were formed outside the pores of the catalysts with higher Ni loading.

The second reduction peak (Fig. 5) at high temperature (about 660 °C) is suggested to be associated with the presence of small NiO particles (smaller than 3 nm in this research) inside the pores of the catalysts at the Ni loadings of 5, 10 and 20 wt.% [29]. These NiO particles have stronger interaction with the support than the bulk NiO particles. The intensity of water generation, detected by MS, showed a similar trend with the intensity of sample weight loss (not shown here).

From the above analysis (SEM, TEM, XRD and TPR) of the fresh Ni/MCM-41 catalysts, NiO particles with a diameter around 3 nm were preferentially located within the pores of the MCM-41 support when the Ni loading was increased from 5 to 20 wt.%. Increasing the Ni loading resulted in NiO particles accumulating outside the pores of the MCM-41 supports and forming bulk particles (200 nm NiO particles for Ni loading up to 40 wt.%).

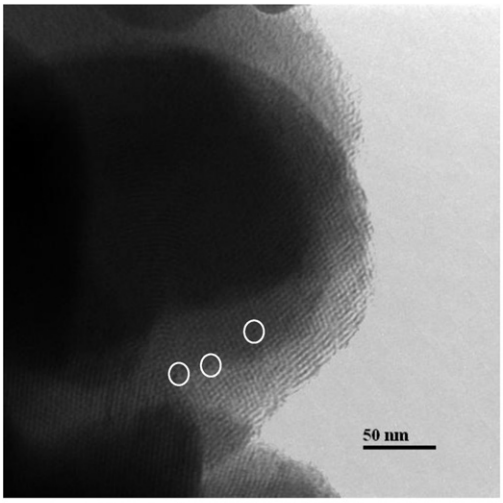

Fresh 5 wt.% Ni/MCM-41

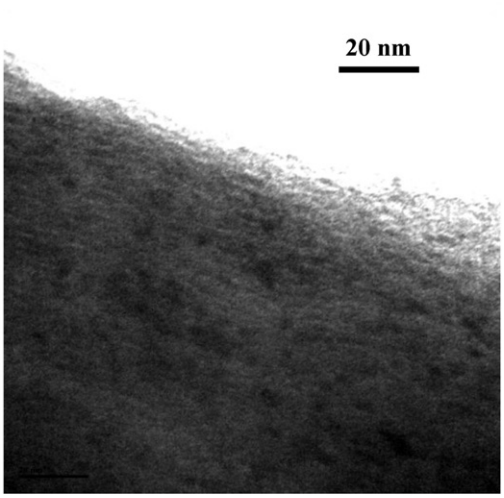

Fresh 20 wt.% Ni/MCM-41

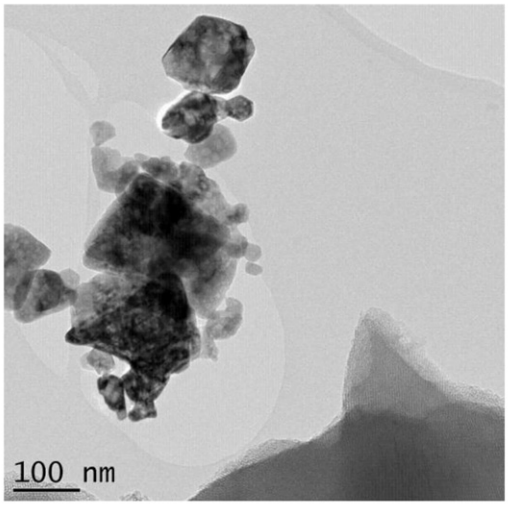

Fresh 40 wt.% Ni/MCM-41

Fig. 4. TEM analysis of the fresh Ni/MCM-41 catalyst.

3.2. Wood sawdust gasification with catalysts

3.2.1. Mass balance

The mass balance of the pyrolysis-gasification of wood sawdust in this research is shown in Table 3. The residue, obtained after pyrolysis, was calculated according to the mass ratio compared to the wood sample. From Table 3, the residue yield was stabilized at around 27 wt.%. The mass balance presented in Table 3 was calculated by the input mass divided by output mass, via the following equation:

$$\text{Mass balance (wt\%)} = \frac{\text{gas mass} + \text{liquid mass} + \text{char mass} + \text{residue mass}}{\text{Wood sawdust mass} + \text{injected water mass}} \times 100$$

The amount of char fraction collected in the reaction tube was negligible. Liquid products were collected in the condensers and were a mixture of oil and non-reacted water. The amount of the injected water was obtained by the mass difference of the water syringe. From Table 3, the experimental results show a reasonable mass balance.

When the gasification was carried out on the catalysts with the loading of Ni ranging from 5 to 40 wt.% the gas yield and hydrogen production were increased. Gas yield related to the mass of wood sample increased from 38.9 to 62.8 wt.% and hydrogen production was increased from 5.6 to 18.2 (mmol H_2 g^{-1} sample), indicating that the Ni loading content on the support plays an important role in the process of biomass gasification. The relation between Ni content and the reactivity of catalysts has been investigated, for example, a Ni/Al_2O_3 catalyst with a Ni content of 15 wt.% was found to possess optimal catalytic activity for tar gasification and increasing the Ni content to 20 wt.% did not show a large difference

Table 3
Mass balance and gas compositions from gasification of biomass.

Catalyst bed	Sand	5 wt.%	10 wt.%	20 wt.%	40 wt.%
Gas/wood (wt.%)	38.9	40.7	46.7	58.1	62.8
Residue/wood (wt.%)	25.9	27.5	25.9	26.2	28.8
Mass balance (wt.%)	100.8	99.2	102.9	102.5	100.4
H_2 yield (mmol H_2 g^{-1} sample)	5.6	6.2	8.3	13.2	18.2
Gas composition (vol.%, N_2 free)					
CO	37.6	38.6	36.2	34.0	26.4
H_2	30.1	31.8	35.2	42.0	50.6
CO_2	12.6	13.0	12.7	13.2	18.4
CH_4	12.1	10.6	9.7	7.6	3.5
C_2–C_4	7.6	6.0	6.2	3.3	1.0

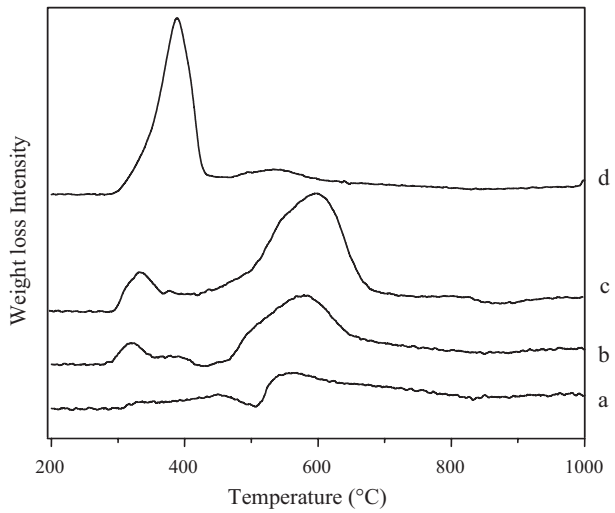

Fig. 5. TPR results of the fresh catalysts; (a): 5 wt.% Ni/MCM-41; (b): 10 wt.% Ni/MCM-41; (c): 20 wt.% Ni/MCM-41; (d): 40 wt.% Ni/MCM-41.

in tar conversion [15]. Using co-precipitated Ni-Al catalyst for the catalytic steam reforming of acetol (one bio-oil model compound from biomass pyrolysis), a Ni-Al catalyst containing 28 mol.% Ni presented a better performance in relation to hydrogen production than that containing 23 mol.% Ni and 33 mol.% Ni at 650 °C [31]. However, increasing the Ni content from 1.5 to 5.7 wt.% for Ni/olivine catalysts enhanced the conversion of toluene reforming [19]. Various Ni loadings from 5 to 20 wt.% for Ni/dolomite did not show a strong influence for toluene steam reforming, a model compound of tar gasification from biomass [15].

It has been proposed that more catalytic nickel sites were available for catalytic gasification to enhance gaseous products, when higher Ni content was loaded on porous supports with higher surface areas. However, the gas and hydrogen production showed little change with the increase of Ni loading from 5 to 10 wt.% on a Ni/CeO_2/ZSM-5 catalyst in the pyrolysis-gasification of polypropylene [32]. It is well known that the high surface areas of zeolites are caused by their micropores rather than their outside surface. Ni particles with sizes of 20 and 30 nm can only locate outside of ZSM-5 with its limited surface area. When an increase of Ni loading from 2 to 5 wt.% was investigated, the dispersion of Ni particles was found to increase on the limited outside surface of ZSM-5 and resulted in increased gas production. Further enhancement of the Ni content resulted in a saturation point of Ni loading being reached on the outside surface and the gas yield could then not be further increased. This phenomenon was also detected on supported Ni-catalysts on mesoporous materials. The gas yield was only slightly changed from 1251 to 1398 ml g^{-1} (only ca. 10% increase) with increasing Ni contents from 5 to 20 wt.% in the steam catalytic gasification of cellulose [22].

However, the gas yield in this research was increased from 38.9 to 62.8 wt.% with the increase of Ni loading from 5 to 40 wt.% on MCM-41, which was contributed by the high dispersion of Ni particles for the gasification of wood sawdust. According to the characterization of the Ni/MCM-41 catalysts, most of NiO particles were smaller than 3 nm inside the mesopores of the 5–20 wt.% Ni/MCM-41 catalysts. Due to the very large internal porous surface areas, these small nano-particles were well dispersed inside the mesopores. Increasing the Ni contents caused an increased number of nano-particles dispersed inside the pores. When the Ni content was up to 20 wt.%, the saturation point of Ni loading inside the pores was reached and Ni particles started to be dispersed on the outside surface of the MCM-41. Further increasing the loading of Ni, the dispersion of Ni particles on the outside surface was increased. It was found that only a few bulk particles on the outside surface of the 20 wt.% Ni/MCM-41 catalyst occurred and much more bulky particles were found when Ni loading was increased as shown by the 40 wt.% Ni/MCM-41 catalyst (Fig. 3). Both small and bulk particles contribute to the biomass gasification process and enhance the gas yield during the reaction.

The highest hydrogen production from gasification of wood sawdust in this research was 18.2 mmol H_2 g^{-1}, which is higher than the 10.5 mmol H_2 g^{-1} produced from the steam catalytic gasification of cellulose on Ni/MCM-41 catalysts [22]. However, there is still a significant potential to increase hydrogen production. The maximum theoretical hydrogen production based on the hydrogen content of the biomass is calculated to be 78.7 mmol H_2 g^{-1}. If it is assumed that 27 wt.% of carbon in the residue is not converted into H_2, then, the maximum hydrogen production is suggested to be about 46.2 mmol H_2 g^{-1}.

3.2.2. Gas concentrations

Gas compositions of CO, H_2, CO_2, CH_4 and C_2–C_4 hydrocarbons for the pyrolysis-gasification of wood sawdust are presented in Table 3. The CO concentration showed a decreasing trend and CO_2 concentration was increased with the increase of Ni loading from 5 to 40 wt.% on the MCM-41 support. The H_2 concentration was increased from 31.8 to 50.6 vol.%, CH_4 concentration was decreased from 10.6 to 3.5 vol.%, and C_2–C_4 concentration was decreased from 6.0 to 1.0 vol.%. It appears that increasing the Ni loading on the Ni/MCM-41 catalyst promoted the water gas shift reaction, where more CO_2 and H_2 were produced. Additionally, gasification of hydrocarbon materials was also promoted with the increase of Ni loading. The CH_4 and C_2–C_4 concentrations were reduced and the H_2 concentration was increased with the increase of Ni content from 2 to 10 wt.% of a Ni/CeO_2/ZSM-5 catalyst, when the catalyst was applied for pyrolysis-gasification of polypropylene [32]. Similar results have also been reported [33,34], when a high Ni loading catalyst was used during the gasification of hydrocarbon materials.

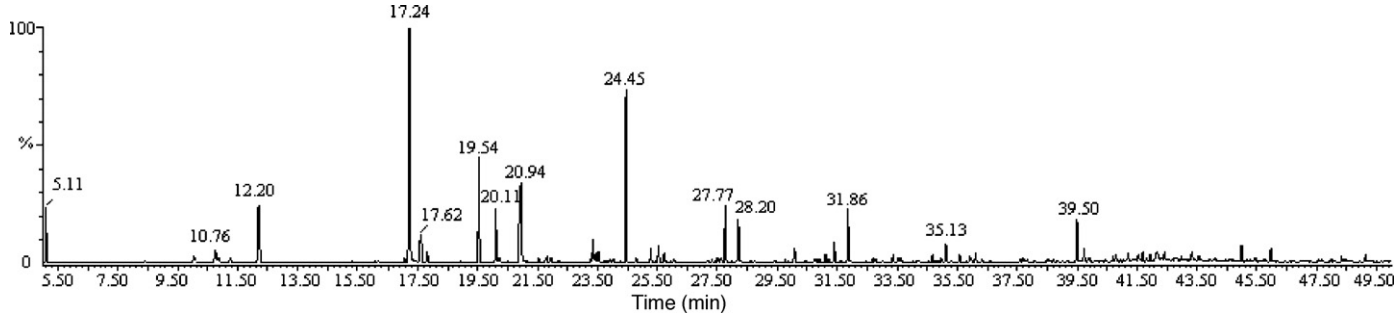

Fig. 6. GC/MS graphic results from steam pyrolysis-gasification of wood sawdust in the absence of Ni/MCM-41 catalyst.

Table 4
Semi-quantitative GC-MS analysis of oil products (Area %).

RT	Name	Sand	5 wt.%	10 wt.%	20 wt.%	40 wt.%
5.11	Toluene	4.3	15.3	22.0	9.8	7.0
10.76	Xylene	1.8	2.6	2.8	2.7	2.3
12.20	Styrene	8.2	9.2	8.0	8.7	13.5
17.24	Phenol	22.9	19.4	17.6	22.6	25.3
17.62	Benzene, 1-ethenyl-3-methyl-	4.5	4.1	2.9	3.4	5.1
19.54	Indene	9.3	6.1	5.3	4.5	5.4
20.11	Phenol, 2-methyl-	4.5	2.2	2.3	2.0	2.5
20.94	Phenol, 4-methyl-	11.3	6.4	6.3	7.5	10.7
24.45	Naphthalene	14.5	17.8	14.8	18.6	13.9
27.77	Benzocycloheptatriene	4.8	4.6	4.2	4.6	2.8
28.20	Naphthalene, 1-methyl-	3.7	3.7	3.5	4.0	5.1
31.86	Biphenylene	4.5	3.7	3.8	3.6	1.8
35.13	Fluorene	2.0	1.6	2.1	2.1	1.0
39.50	Anthracene	3.7	3.4	4.4	5.9	3.7
	Total	100.0	100.0	100.0	100.0	100.0

3.2.3. Bio-oil production

In this research, a valuable bio-oil was produced as a by-product of the pyrolysis-gasification process, which is a benefit in reducing coke generation and enhancing the efficiency of biomass utilisation. Fig. 6 shows a total ion chromatogram (TIC) from the GC/MS analysis of the bio-oil obtained from the steam pyrolysis-gasification of wood sawdust in the presence of sand. Bio-oil containing various compounds was obtained. Table 4 shows the compound retention time, compound name, and mole fraction of bio-oil compounds. The most important and abundant compounds identified are styrene, phenol and naphthalene. These bio-oil compounds have also been identified as the main compounds in the tar derived from pyrolysis of wood samples [35]. Among these compounds, phenols have been reported to be an important commercial product in the pyrolysis oils from straw biomass [36]. The high content of phenol compounds in this research indicates a highly oxygenated product derived from the steam pyrolysis-gasification of wood biomass.

The total TIC peak areas of the identified oils were found to be reduced from 88.7% of total TIC peak areas without catalyst for the gasification on 5 wt.% Ni/MCM-41 catalyst and to 19.3 wt.% of total TIC peak areas without catalyst for that on 40 wt.% Ni/MCM-41 catalyst. It indicates that higher-Ni-loading catalysts with a much higher number of well dispersed NiO particles promoted the conversion of bio-oils to gas products during the gasification of wood sawdust and caused higher hydrogen and total gas yields (Table 3).

3.3. Coke deposition on used catalysts

The reacted catalysts were characterized by TPO analysis and the results are shown in Fig. 7. The curves showed two areas in the TPO analysis: one for Ni particles oxidation, and another for carbon oxidation. The peak of increasing mass (around 300 °C) was associated with the oxidation of Ni during the TPO experiment. The Ni crystal phases were suggested to be produced from the reduction of NiO during the pyrolysis-gasification process, where reducing agents such as CO and H_2 were present, since Ni particles were observed by TEM analysis coupled with energy dispersive X-ray spectroscopy (EDXS) (not shown here). The reduction of NiO during the gasification process has been extensively reported [3,33,37]. It was further shown that Ni particles were found in the reacted catalyst using TEM-EDXS analysis (not shown here). Oxidation of carbon occurred after 550 °C. Filamentous type carbons are known to be formed during the gasification process and have been observed to be oxidized at the temperature of 600 °C during TPO experiments [38,39]. However, filamentous carbons were not confirmed by the SEM analysis in this work (Fig. 8).

The SEM results shown in Fig. 8 were similar for the different reacted Ni/MCM-41 catalysts with different Ni loadings after the pyrolysis-gasification of wood sawdust. However, from the TGA-TPO results (Fig. 7), the amount of coke formation seems to be increased from 0.5 to 4.0 wt.% with the increase of Ni loading from 5 to 40 wt.% on Ni/MCM-41 catalyst, after the pyrolysis-gasification process. The amount of the coke formation was calculated as the weight loss after oxidation of Ni divided by the initial sample weight during the TPO experiment. In this research, the maximum coke deposition was less than 4 wt.% which was obtained for the reacted 40 wt.% Ni/MCM-41 catalyst. It suggests a comparative prohibition of coke formation on the Ni/MCM-41 catalysts prepared in this work during the pyrolysis-gasification of the wood sawdust. More than 10 wt.% of coke deposition was reported on a reacted Ni/Al_2O_3 catalyst for the catalytic steam gasification of biomass by Nishikawa et al. [40].

Coke deposition on the reacted catalyst during the gasification process was reported to poison the active nickel sites and block the pores of the support [41]. The carbon deposition was also suggested to result from growth of Ni particles during tar reduction [20]. Therefore, the increased coke deposition might be due to the increase of NiO particle in the Ni/MCM-41 catalyst when the Ni loading was increased from 5 to 40 wt.%.

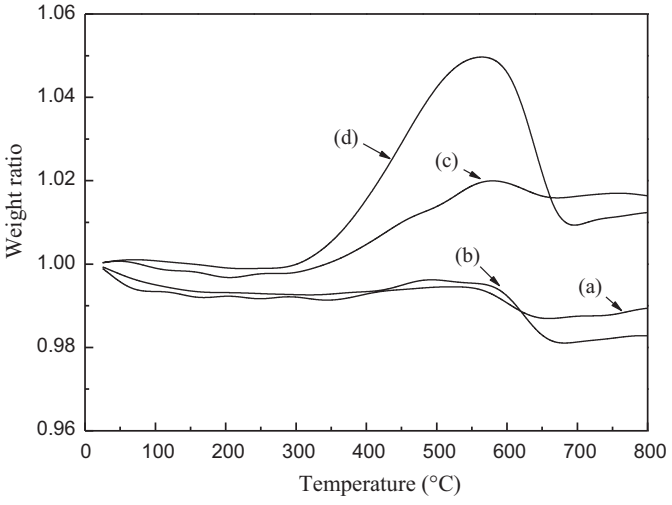

Fig. 7. TPO results of the used catalysts: (a): 5 wt.% Ni/MCM-41; (b): 10 wt.% Ni/MCM-41; (c): 20 wt.% Ni/MCM-41; (d): 40 wt.% Ni/MCM-41.

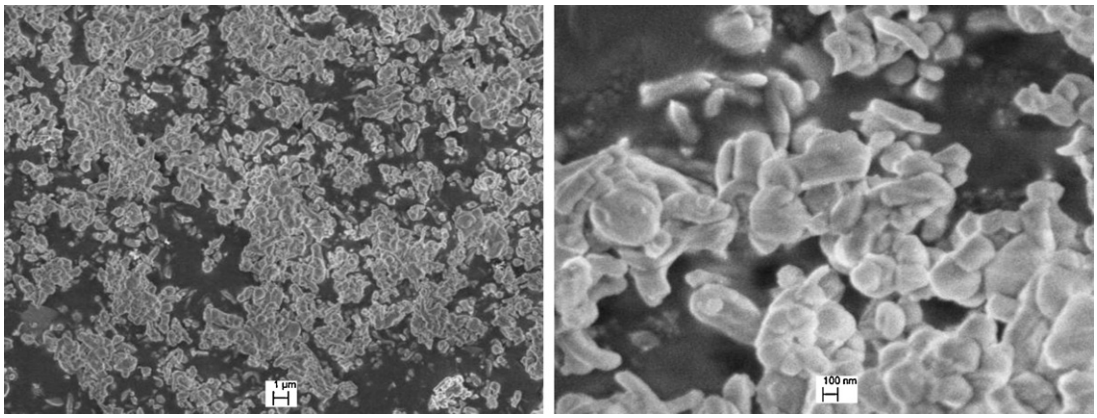

Fig. 8. Typical SEM results of the reacted Ni/MCM-41 catalyst.

4. Conclusions

Hydrogen production from gasification of biomass has been regarded as a promising alternative production technology. In this paper, a Ni catalyst with a high-surface area porous MCM-41 support was investigated for hydrogen production from gasification of wood sawdust. The prepared Ni/MCM-41 catalysts had well-dispersed NiO particles, high surface area, and high pore volume. Most of the Ni particles (less than 3 nm) were located inside the pores of the 5–20 wt.% Ni/MCM-41 catalysts. When the Ni loading was saturated inside the pores, bulk NiO particles (up to 200 nm) were formed on the outside surface of the MCM-41. The well-dispersed NiO particles on MCM-41 supports in this investigation promoted their reactivity in wood sawdust gasification. The experimental results showed that hydrogen and gas yield were increased with the increase of Ni loading from 5 to 40 wt.%. Valuable bio-oil (a mixture of mainly styrene, phenol and other compounds) was produced as by-products, which further contributed to the lowered coke generation (maximum 4% coke generated on catalysts).

Acknowledgements

This work was supported by the UK Engineering and Physical Sciences Research Council under EPSRC grant EP/D053110/1 and the World University Network, Early Career Research Scheme from the University of Sydney.

References

[1] M.A. Dietenberger, M. Anderson, Ind. Eng. Chem. Res. 46 (2007) 8863–8874.
[2] D.K. Liguras, D.I. Kondarides, X.E. Verykios, Appl. Catal. B: Environ. 43 (2003) 345–354.
[3] C. Wu, P.T. Williams, Appl. Catal. B: Environ. 87 (2009) 152–161.
[4] J.B. Gadhe, R.B. Gupta, Ind. Eng. Chem. Res. 44 (2005) 4577–4585.
[5] J. Wang, K. Sakanishi, I. Saito, T. Takarada, K. Morishita, Energy Fuels 19 (2005) 2114–2120.
[6] D. Call, B.E. Logan, Environ. Sci. Technol. 42 (2008) 3401–3406.
[7] P. Lv, J. Chang, T. Wang, Y. Fu, Y. Chen, Energy Fuels 18 (2004) 228–233.
[8] S. Albertazzi, F. Basile, J. Brandin, J. Einvall, C. Hulteberg, G. Fornasari, V. Rosetti, M. Sanati, F. Trifiro, A. Vaccari, Catal. Today 106 (2005) 297–300.
[9] R. Muangrat, J.A. Onwudili, P.T. Williams, Appl. Catal. B: Environ. 100 (2010) 440–449.
[10] R. Muangrat, J.A. Onwudili, P.T. Williams, Appl. Catal. B: Environ. 100 (2010) 143–156.
[11] I. Hannula, E. Kurkela, Biomass Bioenergy 101 (2010) 4608–4615.
[12] Y.J. Lu, S. Li, L.J. Guo, X.M. Zhang, Int. J. Hydrogen Energy 35 (2010) 7161–7168.
[13] Y. Richardson, J. Blin, G. Volle, J. Motuzas, A. Julbe, Appl. Catal. A: Gen. 382 (2010) 220–230.
[14] T. Kimura, T. Miyazawa, J. Nishikawa, S. Kado, K. Okumura, T. Miyao, S. Naito, K. Kunimori, K. Tomishige, Appl. Catal. B: Environ. 68 (2006) 160–170.
[15] J. Srinakruang, K. Sato, T. Vitidsant, K. Fujimoto, Catal. Commun. 6 (2005) 437–440.
[16] T. Miyazawa, T. Kimura, J. Nishikawa, S. Kado, K. Kunimori, K. Tomishige, Catal. Today 115 (2006) 254–262.
[17] T. Furusawa, A. Tsutsumi, Appl. Catal. A: Gen. 278 (2005) 207–212.
[18] T.J. Wang, J. Chang, C.Z. Wu, Y. Fu, Y. Chen, Biomass Bioenergy 28 (2005) 508–514.
[19] D. Swierczynski, S. Libs, C. Courson, A. Kiennemann, Appl. Catal. B: Environ. 74 (2007) 211–222.
[20] P.R. Buchireddy, R.M. Bricka, J. Rodriguez, W. Holmes, Energy Fuels 24 (2010) 2707–2715.
[21] M. Inaba, K. Murata, M. Saito, I. Takahara, Energy Fuels 20 (2006) 432–438.
[22] M. Zhao, N.H. Florin, A.T. Harris, Appl. Catal. B: Environ. 92 (2009) 185–193.
[23] M. Zhao, N.H. Florin, A.T. Harris, Appl. Catal. B: Environ. 97 (2010) 142–150.
[24] C.F. Cheng, D.H. Park, J. Klinowski, J. Chem. Soc. Faraday Trans. 93 (1997) 193–197.
[25] Y.S. Cho, J.C. Park, B. Lee, Y.H. Kim, J. Yi, Catal. Lett. 81 (2002) 89–96.
[26] D.J. Lensveld, J.G. Mesu, A.J. Dillen, K.P. Jong, Microporous Mesoporous Mater. 44 (2001) 401–407.
[27] G. Li, L. Hu, J.M. Hill, Appl. Catal. A: Gen. 301 (2006) 16–24.
[28] A. Szegedi, M. Popova, V. Mavrodinova, M. Urbán, I. Kiricsi, C. Minchev, Microporous Mesporous Mater. 99 (2007) 149–158.
[29] A.M. Diskin, R.H. Cunningham, R.M. Ormerod, Catal. Today 46 (1998) 147–154.
[30] W.S. Dong, H.S. Roh, K.W. Jun, S.E. Park, Y.S. Oh, Appl. Catal. A: Gen. 226 (2002) 63–72.
[31] F. Bimbela, M. Oliva, J. Ruiz, L. Garcia, J. Arauzo, J. Anal. Appl. Pyrolysis 85 (2009) 204–213.
[32] C. Wu, P.T. Williams, Int. J. Hydrogen Energy 34 (2009) 6242–6252.
[33] C. Wu, P.T. Williams, Appl. Catal. B: Environ. 90 (2009) 147–156.
[34] K. Tomishige, T. Kimura, J. Nishikawa, T. Miyazawa, Catal. Commun. 8 (2007) 1074–1079.
[35] P. Gilbert, C. Ryu, V. Sharifi, J. Swithenbank, Bioresour. Technol. 100 (2009) 6045–6051.
[36] F. Ateş, M.A. Işikdağ, Energy Fuels 22 (2008) 1936–1943.
[37] O. Clause, M. Gazzano, F. Trifiro, A. Vaccari, L. Zatorski, Appl. Catal. 73 (1991) 217–236.
[38] C. Wu, P.T. Williams, Appl. Catal. B: Environ. 96 (2010) 198–207.
[39] S. Wang, G.Q. Lu, Ind. Eng. Chem. Res. 38 (1999) 2615–2625.
[40] J. Nishikawa, T. Miyazawa, K. Nakamura, M. Asadullah, K. Kunimori, K. Tomishige, Catal. Commun. 9 (2008) 195–201.
[41] J. Scherzer, A.J. Gruia, Hydrocracking Science and Technology, Taylor & Francis, Inc., Oxford, UK, 1996.